

Atomic imaging of atomic layer deposition oxide nucleation with trimethylaluminum on As-rich InGaAs(001) 2×4 vs Ga/In-rich InGaAs(001) 4×2

Wilhelm Melitz, Tyler Kent, Andrew C. Kummel, Ravi Droopad, Martin Holland, and Iain Thayne

Citation: *The Journal of Chemical Physics* **136**, 154706 (2012); doi: 10.1063/1.4704126

View online: <http://dx.doi.org/10.1063/1.4704126>

View Table of Contents: <http://scitation.aip.org/content/aip/journal/jcp/136/15?ver=pdfcov>

Published by the [AIP Publishing](#)

Articles you may be interested in

Synchrotron radiation photoemission study of interfacial electronic structure of HfO₂ on In_{0.53}Ga_{0.47}As(001)- 4×2 from atomic layer deposition

Appl. Phys. Lett. **104**, 042904 (2014); 10.1063/1.4863440

Effective passivation of In_{0.2}Ga_{0.8}As by HfO₂ surpassing Al₂O₃ via in-situ atomic layer deposition

Appl. Phys. Lett. **101**, 172104 (2012); 10.1063/1.4762833

Atomic imaging of the monolayer nucleation and unpinning of a compound semiconductor surface during atomic layer deposition

J. Chem. Phys. **133**, 154704 (2010); 10.1063/1.3487737

Arsenic decapping and half cycle reactions during atomic layer deposition of Al₂O₃ on In_{0.53}Ga_{0.47}As (001)

Appl. Phys. Lett. **96**, 252907 (2010); 10.1063/1.3452336

Pre-atomic layer deposition surface cleaning and chemical passivation of (100) In_{0.2}Ga_{0.8}As and deposition of ultrathin Al₂O₃ gate insulators

Appl. Phys. Lett. **93**, 052911 (2008); 10.1063/1.2966357



2014 Special Topics

PEROVSKITES

2D MATERIALS

MESOPOROUS MATERIALS

BIOMATERIALS/ BIOELECTRONICS

METAL-ORGANIC FRAMEWORK MATERIALS

AIP | APL Materials

Submit Today!

Atomic imaging of atomic layer deposition oxide nucleation with trimethylaluminum on As-rich InGaAs(001) 2×4 vs Ga/In-rich InGaAs(001) 4×2

Wilhelm Melitz,^{1,2} Tyler Kent,^{1,2} Andrew C. Kummel,^{2,a)} Ravi Droopad,³ Martin Holland,⁴ and Iain Thayne⁴

¹Materials Science and Engineering Program, University of California, San Diego, La Jolla, California 92093, USA

²Department of Chemistry and Biochemistry, University of California, San Diego, La Jolla, California 92093, USA

³Department of Physics, Texas State University, San Marcos, Texas 78666, USA

⁴Department of Electronics and Electrical Engineering, University of Glasgow, Glasgow, G12 8LT, Scotland, United Kingdom

(Received 20 January 2012; accepted 31 March 2012; published online 19 April 2012)

Formation of a contaminant free, flat, electrically passive interface to a gate oxide such as a-Al₂O₃ is the critical step in fabricating III-V metal oxide semiconductor field effect transistors; while the bulk oxide is amorphous, the interface may need to be ordered to prevent electrical defect formation. A two temperature *in situ* cleaning process is shown to produce a clean, flat group III or group V rich InGaAs surface. The dependence of initial surface reconstruction and dosing temperature of the seeding of aluminum with trimethylaluminum dosing is observed to produce an ordered unpinned passivation layer on InGaAs(001)-(4 × 2) surface at sample temperatures below 190 °C. Conversely, the InGaAs(001)-(2 × 4) surface is shown to generate an unpinned passivation layer with a seeding temperature up to 280 °C. For both reconstructions, the chemical drive force is consistent with formation of As-Al-As bonds. The optimal seed layer protects the surface from background contamination.

© 2012 American Institute of Physics. [<http://dx.doi.org/10.1063/1.4704126>]

INTRODUCTION

III-V semiconductors² and high-k oxides for metal oxide semiconductor field effect transistors (MOSFETs) are an alternative/complementary technology to traditional silicon MOSFETs because of their potentially high drive currents at low source-drain voltage.¹ To enable low power MOSFET operation, there are several requirements: (1) The MOSFET must have a low gate voltage which requires a small equivalent oxide thickness (EOT), below 1 nm, so the oxide growth must be nucleated in each unit cell. (2) The semiconductor channel must have a high mobility and high saturation velocity so the oxide-semiconductor interface must be extremely flat. (3) The subthreshold swing must be close to ideal which necessitates a low interfacial trap density (D_{it}) so the oxide-semiconductor interfaces must have a low defect density. To form a low defect oxide/III-V interface, the semiconductor surface may need to be clean prior to oxide nucleation and the oxide-semiconductor interface may need be ordered to minimize defect formation. (4) Remote phonon scattering needs to be minimized which is usually achieved by having the first gate oxide layer be ALD deposited amorphous Al₂O₃.²

Surface channel III-V MOS devices can be fabricated with atomic layer deposition (ALD) high-K gate-first processes³⁻⁶ which are similar to SiO₂ growth on silicon or ALD of high-K on silicon.⁷⁻¹¹ The key for a gate-first process is that subsequent processing steps cannot degrade the

semiconductor, the dielectric, or the oxide-semiconductor interfaces. For silicon, the only commercial ALD high-k fabrication process is a replacement gate process (a type of gate-last process) to avoid processing induced damage.¹² Some work has been reported on replacement gates on III-Vs.¹³ While preparing silicon for gate-last processing is straightforward, preparing an ordered clean III-V semiconductor surface for gate-last processing is a challenge. It has been shown that ALD of trimethylaluminum (TMA)^{14,15} or tetrakis(ethylmethylamino)hafnium¹⁶ on III-V has self-cleaning properties by reducing the presence of As-O and Ga-O bonds. Recently, a combination of atomic hydrogen and TMA has shown an improvement of the D_{it} over just traditional TMA cleaning.¹⁷ However, for high quality dielectric semiconductor interfaces, further reduction or cleaning of native oxide may be required and the interface must be atomically flat. Furthermore, aggressive oxide thickness reduction (equivalent oxide thickness or EOT scaling) is needed to fabricate small gate length devices with small subthreshold swings, and aggressive EOT scaling requires a very uniform ALD nucleation density with no pinholes.¹⁸ The key barrier to a very practical problem is a simple surface chemistry challenge: development of a chemical process, which removes nearly all air induced defects and contaminants and leaves the III-V surface flat and electrically active for high nucleation density ALD gate oxide deposition, which unpins the Fermi level.

This study investigates the surface preparation for ALD of Al₂O₃ on In_{0.53}Ga_{0.47}As via atomic hydrogen cleaning and

^{a)} Author to whom correspondence should be addressed. Electronic mail: akummel@ucsd.edu.

the initial passivation and gate oxide nucleation via TMA. It has been previously shown that atomic hydrogen cleaning can produce In/Ga-rich InGaAs surface with defect densities similar to decapped samples;¹⁹ here it will be shown that the As-rich surface can also be produced with atomic hydrogen cleaning with low defect density and an unpinned electronic structure. Using *in situ* scanning tunneling microscopy (STM) and scanning tunneling spectroscopy (STS), the nucleation properties and electronic structure of TMA of hydrogen cleaned/annealed InGaAs(001)-(2 × 4) and (4 × 2) surfaces are compared on the atomic scale as a function of dosing temperatures. MOSCAP studies by Hwang *et al.* have shown that TMA based a-Al₂O₃ oxide growth at elevated temperature on 2 × 4 produces a lower D_{it} in comparison to the TMA dosing at elevated temperature on 4 × 2.²⁰ Although the 2 × 4 surface may be more prone to formation of As oxides during ALD oxide growth, TMA is known to bond strongly to As atoms and therefore to be more efficient for reducing As₂O₃ formation than reducing Ga or In oxide formation.^{21,22} The present study probes the initial bonding of TMA on the 2 × 4 and 4 × 2 surfaces as a function of temperature to determine if the formation of the initial monolayer determines the differences in electronic properties of gate oxides grown on these two reconstructions. By understanding the ordered bonding of TMA on different reconstructions, the mechanism of chemical passivation and electronic passivation can be elucidated for TMA on III-V surfaces. For both the As-rich 2 × 4 and the In/Ga rich 4 × 2 reconstructions, the bonding of the TMA reactions products and the passivation of the dangling bonds is consistent with the chemical driving force being the formation of As-Al-As bonds.

EXPERIMENTAL SETUP

In the present study, two sample types were employed. The “capped” samples have an As₂ cap on a 0.2 μm thick In_{0.53}Ga_{0.47}As layer grown by MBE on commercially available InP wafers. The MBE-grown InGaAs layers are doped *n*-type and *p*-type with a doping concentration of 2 × 10¹⁸ cm⁻³ of Si and Be dopants. Following MBE growth, the samples are capped with a 50 nm As₂ layer and shipped/stored under vacuum before being loaded into the Ultra-high vacuum (UHV) chamber. The As₂ capped samples allow for comparison of pristine samples to air exposed/H cleaned samples. The “uncapped” samples have a 0.05 μm thick In_{0.53}Ga_{0.47}As layer grown by MBE on commercially available InP wafer, without an As₂ cap. The uncapped samples are shipped/stored in air. The samples are loaded into an Omicron UHV chamber with base pressure below 1 × 10⁻¹⁰ Torr.

Capped samples are decapped in UHV at 330–360 °C and annealed to 380–420 °C or 450–470 °C to form the InGaAs(001)-(2 × 4) or (4 × 2) surface reconstructions. Further details concerning the decapped samples and preparation methods are published in Refs. 19 and 23. The uncapped samples are cleaned with atomic hydrogen in UHV using an Oxford Applied Research TC-50 thermal gas cracker in the preparation chamber at optimized sample temperatures and dose times with a H₂ pressure of 1–2 × 10⁻⁶ Torr.¹⁹ To form the As-rich InGaAs(001)-(2 × 4) surface reconstruc-

tion, the atomic hydrogen cleaning and post deposition annealing is performed at 270–290 °C. To form the In/Ga rich InGaAs(001)-(4 × 2), a higher temperature atomic hydrogen cleaning at 380–400 °C is performed followed by a post-deposition anneal to 450–470 °C. Further details of atomic hydrogen cleaning to achieve the InGaAs(001)-(4 × 2) surface have been previously reported.¹⁹

After decapping or surface cleaning, the samples are transferred *in situ* to an analysis chamber containing an Omicron variable temperature atomic force/scanning tunneling microscopy (AFM/STM) with a base pressure of 2 × 10⁻¹¹ Torr. STM provides atomic resolution of the surface morphology while STS^{24–27} is performed to determine the electrical quality of the surface. STS studies show that the clean InGaAs(001)-(4 × 2) surface reconstruction is pinned consistent with the presence of strained In/Ga dimers,^{19,23,28} therefore, to show the surface will be unpinned upon suitable oxide deposition, surface passivation is required. Auger electron spectroscopy (AES) was also performed in the preparation chamber using a Phi 10–155 cylindrical-Auger spectrometer.

TMA is synergistic because it electrically passivates the surface, chemically passivates (i.e., protects the surface against oxidation), and provides a monolayer nucleation density required for very thin gate oxide formation.²² The deposition of TMA is performed in the load lock, again allowing for sample transfer *in situ*. The load lock is first baked overnight until it reaches a base pressure below 1 × 10⁻⁷ Torr to avoid water contamination (commercial ALD tools employ hot walls, which is a similar but faster technique). The sample is exposed to 1 × 10⁻⁶ – 1 × 10⁻² Torr of TMA vapor for 5 s at a fixed temperature. The samples are transferred into the preparation chamber for PDA and AES. The samples are transferred back into the load lock where they are exposed to ~10 000 L of O₂, by leaking in a diluted gas mixture of 20% O₂ in helium.

RESULTS AND DISCUSSION

STM of TMA on In/Ga-rich InGaAs(001)-(4 × 2) and As-rich InGaAs(001)-(2 × 4)

Figure 1(a) shows the STM image of the decapped InGaAs(001)-(4 × 2) surface. A similar surface can be formed with atomic hydrogen cleaning of air exposed surfaces at 380 °C followed by a PDA to 450–470 °C. The clean InGaAs(001)-(4 × 2) surface contains In/Ga dimers along with some defects, bright rows²⁹ indicated by an oval and dark rows³⁰ indicated by a rectangle in Figure 1(a). After the InGaAs(001)-(4 × 2) surface is exposed to TMA vapor < 1 × 10⁻³ Torr for 5–10 s with a sample temperature 24–190 °C, the surface undergoes an adsorbate induced surface reconstruction, details of this reconstruction can be seen in previously published results.²² This low temperature TMA dosed surface exhibits a 90° rotation in the surface rows, and has row spacing is 0.8 nm, as shown in Figure 1(b). The TMA surface reconstruction demonstrates high nucleation density and self-limiting behavior, ideal for aggressive EOT scaling. However, the surface passivation is quite different from the typical temperatures employed for Al₂O₃ ALD, 270–300 °C.^{17,20,31} If the InGaAs(001)-(4 × 2) surface is

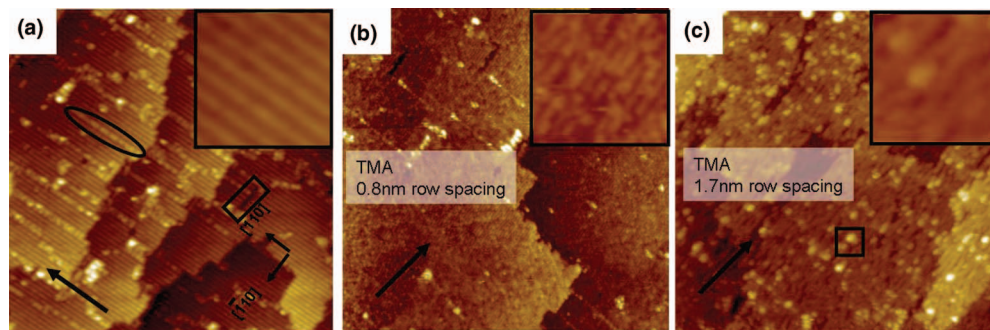


FIG. 1. Filled state STM images ($100 \times 100 \text{ nm}^2$) (a) decapped InGaAs(4×2). Oval indicates bright defects, rectangle indicates dark defects. Arrow indicates row direction. (b) $\sim 1000 \text{ L}$ room temperature dose of TMA @ $P = 1e^{-4}$ Torr on the 4×2 surface showing a 90° change in the surface order with 0.8 nm spaced rows, indicated by arrow. This surface structure is observed for dosing temperatures from room temperature to 190°C . (c) $\sim 1000 \text{ L}$ 280°C TMA dose @ $P = 1e^{-4}$ Torr and anneal to 290°C on 4×2 surface showing the same 90° change with increase row spacing of 1.7 nm . Insets are $10 \times 10 \text{ nm}^2$ STM images of respective images. Black square indicates bright features, most likely second layer growth.

exposed to TMA vapor $< 1 \times 10^{-3}$ Torr for 5–10 s with a sample temperature above 250°C , the surface again undergoes 90° change in row direction; however, the row spacing is doubled to 1.7 nm , Figure 1(c). For the higher temperature TMA dosed surface, some second layer growth is observed. A black square in Figure 1(c) indicates a bright feature in STM that is consistent with second layer growth.

To further illustrate the difference between the two TMA surface reconstructions, higher resolution STM images are shown in Figure 2. Figure 2(a) shows the lower temperature dosing with the self-limiting highly ordered adsorbate structure and a high nucleation density with 0.8 nm row spacing. While this high density passivation is ideal, this deposition process would require two temperature processing since typically Al_2O_3 ALD temperature is $270\text{--}300^\circ \text{C}$. On the 280°C TMA dosed surface, Figure 2(b), the TMA still exhibits the

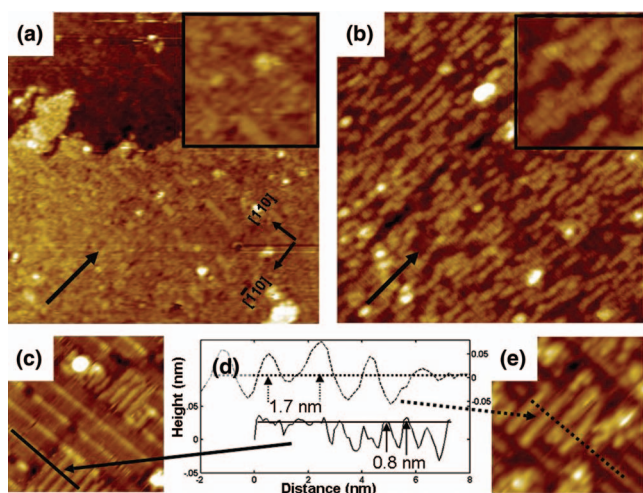


FIG. 2. Filled state STM images ($50 \times 50 \text{ nm}^2$) (a) $\sim 1000 \text{ L}$ 190°C dose of TMA @ $P = 1e^{-4}$ Torr on the 4×2 surface showing an ordered surface with 0.8 nm spaced rows, row direction indicated by arrow. (b) $\sim 100 \text{ L}$ 250°C TMA dose @ $P = 1e^{-4}$ Torr on 4×2 surface showing an ordered surface with increased row spacing of 1.7 nm . The arrow indicates row direction. Insets are $10 \times 10 \text{ nm}^2$ STM images of respective images. (c) Low coverage TMA dose on 4×2 dosed at room temperature and annealed to 200°C . (d) Line traces for low coverage scans. Solid line for the room temperature dose and anneal to 200°C . Dotted line for the room temperature dose and anneal to 300°C . (e) Low coverage TMA dose on 4×2 dosed at room temperature and annealed to 300°C .

self-limiting highly order adsorbate structure, just with wider spacing. Figures 2(c) and 2(e) show low coverage images of the low and high temperature TMA structures on the 4×2 surface. Besides the spacing being different between the low and high temperature structures, the high temperature structure is $\sim 0.05 \text{ nm}$ taller than the In/Ga 4×2 rows, while the low temperature structure is the same height as the In/Ga 4×2 rows.

The InGaAs(001)-(2×4) surface contains As-dimers, and the surface has a low defect density in contrast to the 4×2 surface. Figure 3(a) shows a decapped InGaAs(001)-(2×4) with the classic zig-zag structure which is a mixture

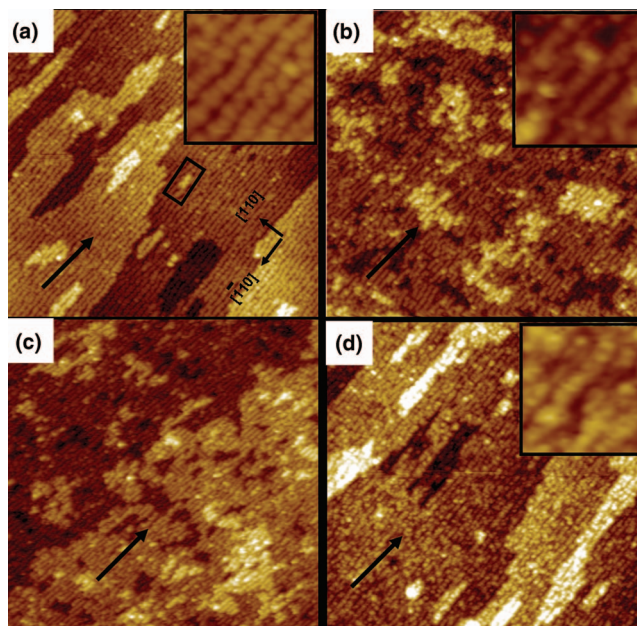


FIG. 3. Filled state STM images ($100 \times 100 \text{ nm}^2$) (a) decapped InGaAs(2×4) (b) uncapped InGaAs sample annealed for 30 min at 280°C followed by 30 min hydrogen (1800 L) dose at 285°C . (c) After post-deposition anneal at 290°C for 30 min. (d) After a $\sim 1000 \text{ L}$ dose of TMA at 285°C , the surface shows similar structure as decapped 2×4 surface. The ordered TMA surface is seen over a wide range of temperatures ($24\text{--}285^\circ \text{C}$) and pressures ($5e^{-6}\text{--}1e^{-3}$ Torr), and a low dangling bond density is observed with the doses $> 1e^{-4}$ Torr. At much higher pressures the surface looks amorphous. While the 2×4 row direction and symmetry are preserved, the row structure is modified. The arrows indicate row direction. A bright defect or small terrace is in side black rectangle.

of single and double As-dimers.²³ The 2×4 surface does contain some narrow terraces indicated in rectangular box in Figure 3(a). The As-rich 2×4 can be formed from an air exposed surface by lowering the atomic hydrogen cleaning temperature to 280 °C, Figure 3(b). The atomic hydrogen cleaned surface shows more surface roughness than the decapped surface which is not ideal for high mobility channels. However, it may be possible to form lower roughness surfaces with optimization of the dosing and annealing times and temperatures. Lower roughness was observed with a PDA at 280 °C, Figure 3(c), but the roughness reduction via PDA was greater on the 4×2 surface. Atomic hydrogen has been shown to convert atomic As and As_2O_3 into AsH_3 and/or H_2O .³² The high temperature hydrogen cleaning producing the In/Ga rich surface is consistent with atomic hydrogen at around 400 °C removing As on GaAs^{33;34} as well as the desorption of As oxides and As_2/As_4 occurs around 400 °C.^{33;34} The low temperature hydrogen cleaning forming the clean As-rich 2×4 surface implies that hydrogen does not react with As at 280 °C but the hydrogen still reduces the In, Ga, and As oxides to 280 °C.

After the $\text{InGaAs}(001)-(2 \times 4)$ is exposed to TMA vapor $< 1 \times 10^{-3}$ Torr for 5–10 s at a sample temperature of 24 °C or 280 °C, the surface maintains its row direction, but loses the zig-zag characteristic seen on the clean 2×4 surface, Figure 3(d). The TMA dosed on the 2×4 surface shows high nucleation density and self-limiting behavior, i.e., no second

layer growth. This implies that in contrast to the 4×2 surface, the As rich 2×4 surface can be cleaned and functionalize at maximum density at 280 °C which is the typical growth temperature of ALD Al_2O_3 gate oxide. The wider temperature range for maximum density TMA chemisorption on the 2×4 surface is consistent with the 2×4 surface having As-As dimers (382.0 ± 10.5 kJ mol⁻¹, the bonding enthalpies used are from the gas phase) which should strongly bond to the aluminum atom, Al-As (202.9 ± 10.5 kJ mol⁻¹) in the expected dissociative chemisorption product, dimethyl aluminum since one As-As bond will be replaced with two As-Al bonds in $\text{As-Al}(\text{CH}_3)_2\text{-Al}$ bonding geometry.³⁵

Figure 4 illustrates possible bonding models for the clean and TMA dosed surfaces for both the 4×2 and 2×4 reconstructions. One model of the clean 4×2 contains a In/Ga row with In/Ga-dimers in the trough,^{28,36} Figure 4(a). The TMA dosed and annealed below 190 °C induce a surface reconstruction that rotates the row order 90° with 0.8 nm row spacing,²² shown in Figure 4(b). At a higher dosing or annealing temperatures, it is hypothesized that some methyl groups desorb leaving dangling bonds on the aluminum atoms. Another model of the clean 4×2 surface is shown in Figure 4(d) based on a model for InAs and InSb 4×2 .^{37,38} The respective model for the TMA dosed and annealed surface below 190 °C again induces a surface reconstruction to generate a row order of 90° with 0.8 nm row spacing, Figure 4(e). Furthermore, at higher dosing or annealing temperatures some

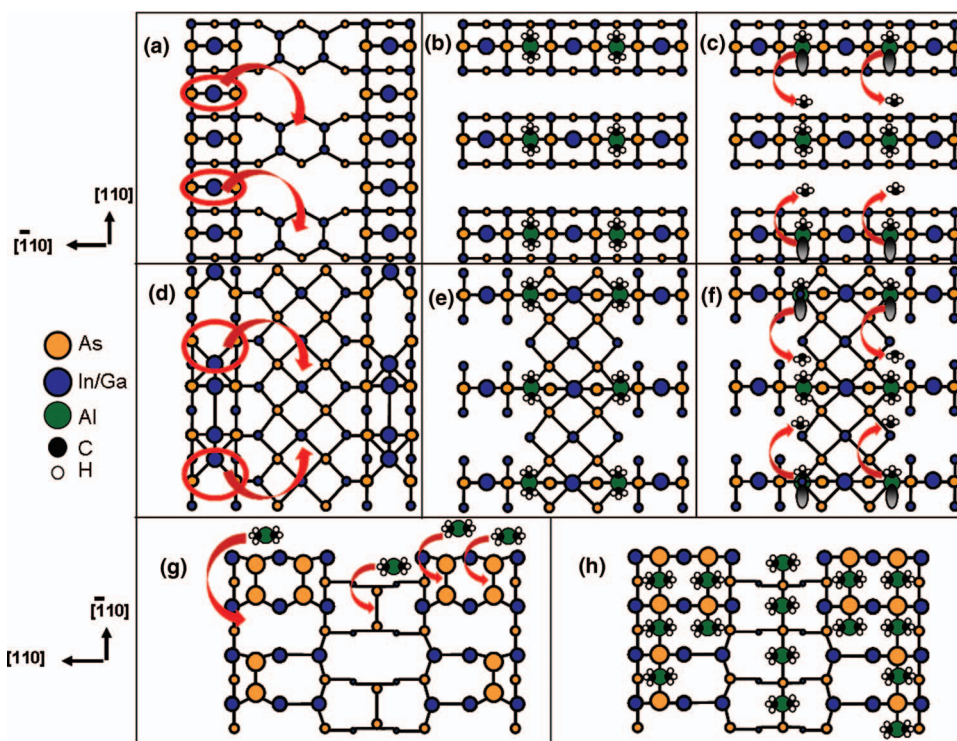


FIG. 4. Ball-and-stick diagram based on the model from Feldwinn *et al.*³⁶ of (a) the clean 4×2 surface, (b) the adsorbate induced reconstruct of TMA dosed below 190 °C on 4×2 and annealed,²² (c) a possible model of the higher temperature adsorbate induced reconstruct of TMA on the 4×2 reconstruction containing dangling bonds. Ball-and-stick diagram based on the model from Goryl *et al.*³⁷ and Kumpf *et al.*³⁸ of (d) the clean 4×2 surface, (e) a possible adsorbate induced reconstruct of TMA dosed below 190 °C on 4×2 and annealed, (f) a possible model of the higher temperature adsorbate induced reconstruct of TMA on 4×2 containing dangling bonds. Ball-and-stick diagram based on the model from Shen *et al.*²³ of (g) the clean 2×4 surface with double or single dimer unit cells, and (h) the TMA dosed surface on the double or single dimer unit cells. Note it is possible CH_3 groups may also be adsorbed on the surface. The red oval and arrow illustrates the movement of As-In-As row atoms to the trough. Other arrows indicate either chemisorption of DMA or desorption of a methyl group.

methyl groups desorb leaving dangling bonds. The dimethyl-aluminum bonded to the surface is tetrahedral coordinated; therefore, if a methyl desorbs, the dangling bond should be directed along the [110] direction. In STM, row spacing of 1.7 nm are observed suggesting the dangling bonds occurring every other row. The rows on the high temperature TMA dosed 4×2 shown in Figure 2(d) are ~ 0.05 nm taller than the In/Ga rows and have a row spacing of 1.7 nm. Further experiments or calculations are needed to support this model. However, the presence of dangling bonds for the high temperature TMA dosed 4×2 surface is consistent with the pinned electronic structure as shown below. The clean 2×4 surface contains rows of single or double As-dimers,²³ Figure 4(g). It is hypothesized that the aluminum atom in the TMA chemisorption product breaks the As-dimers to form two Al-As bonds; this would also generate a high nucleation density of Al on the surface as shown in Figure 4(h).

STS of TMA on InGaAs(001) (4×2) vs (2×4)

The STS spectra for clean n-type and p-type InGaAs(001)-(4×2) as shown in Figures 5(a) and 5(b). For the decapped surface (solid blue curves), Fermi level on both the n-type and p-type samples is positioned near the valence band (VB) indicating the decapped surface is pinned. For InGaAs, it is common that the Fermi level is pinned near the conduction band edge;³⁹ however, STS is a conductance based technique and will ignore fixed charge or deep traps, a more detailed analysis of this topic can be seen in Ref. 40. After TMA dosing of the n-type InGaAs(001)-(4×2) surface at 190°C , the spectra for n-type shifts relative to the pinned clean surface; for the 190°C TMA dose surface, the Fermi level on n-type is near the conduction band edge while on p-type it is near the valence band edge consistent

with an unpinned interface. Conversely, after TMA dosing on the n-type InGaAs(001)-(4×2) surface at 240°C , the spectra is similar to the decapped surface consistent with pinning. The data are consistent with the existence of a maximum dosing temperature for formation of a good electrical interface between the clean 4×2 and the initial seed layer of TMA. This difference correlates with the different adsorbate induced surface reconstructions: the unpinned 0.8 nm spacing TMA and the pinned 1.7 nm spacing TMA reconstruction. The spectra suggest that the initial seed layer needs to be performed at lower temperatures to achieve an unpinned interface, requiring a change in sample temperatures in the oxide growth.

The spectra for the 2×4 surface suggest a different trend. Figures 5(c) and 5(d) show the spectra for n-type and p-type InGaAs(001)-(2×4). On the decapped 2×4 surface (solid blue curves), the surface Fermi level for n-type is near the conduction band and near the VB for p-type consistent with the surface being unpinned. After TMA dosing on the n-type InGaAs(001)-(2×4) at 280°C , the surface Fermi level remains approximately in the same position, suggesting the TMA leaves the surface unpinned. The spectra are consistent with the initial TMA seed layer maintaining an unpinned surface at higher temperature consistent with the strong bonding the TMA chemisorption product to the As-As dimers.

AES of initial passivation of InGaAs(001) (4×2) vs (2×4)

Table I shows the atomic ratios of relative concentrations of the C, O, and Al for the clean and dosed InGaAs(001)-(4×2) surfaces, see supplementary material for corresponding AES spectra.⁴² Using the intensity of the major auger transition peak, the atomic ratios can be estimated.⁴¹ For the LMM

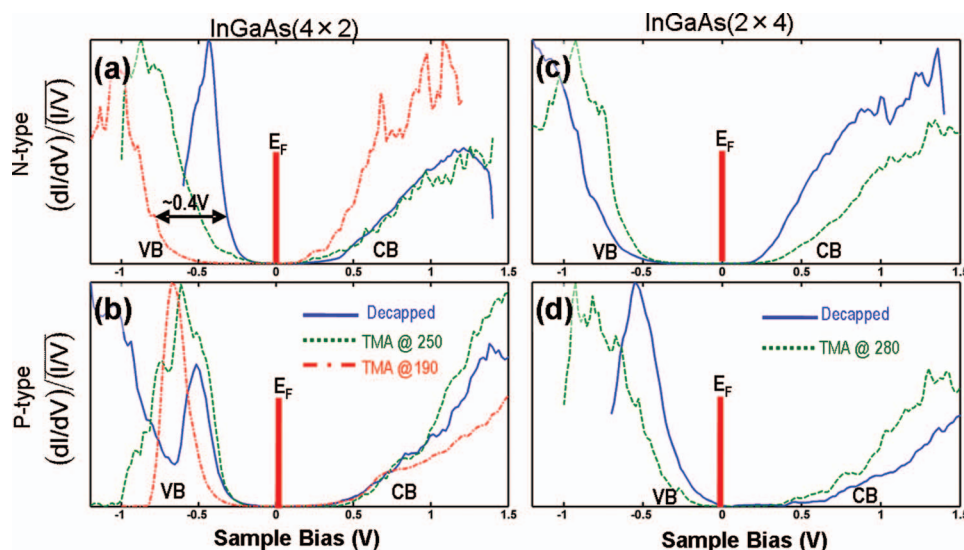


FIG. 5. STS spectra for the TMA dosing on InGaAs 4×2 and 2×4 at various temperatures. (a) Spectra for n-type InGaAs 4×2 showing both the decapped and 250°C TMA dose have a surface Fermi level near the valence band (VB) while the TMA dosed at 190°C surface are near the conduction band (CB). (b) All the spectra show the surface Fermi levels are near the VB. The 4×2 spectra indicate the TMA surface reconstruction at 190°C with 0.8 nm spacing are unpinned while the TMA dosed surfaces at temperatures above 250°C with 1.7 nm spacing are pinned. (c) Spectra for n-type InGaAs 2×4 showing both the decapped and 280°C TMA dose have a surface Fermi level near the CB. (d) Both the decapped and 280°C TMA dosed surface Fermi levels are near the VB. The 2×4 spectra indicate the TMA leaves the surface unpinned over a wider processing window.

TABLE I. AES atomic ratios for InGaAs(001)-(4 × 2) surface and dosed surfaces. The values are the average of four fittings of the Al peak, either normalized to the In peak or a low energy Ga peak. The percent does not correspond to the fraction of a monolayer but instead is the percent of the total Auger signal from In, Ga, As, Al, C, and O. All clean surfaces show an atomic concentration of carbon <3% and oxygen <1% demonstrating the initial surface is extremely clean. It is noted that the carbon and oxygen levels are a function of Auger spectroscopy conditions since the Auger electron gun deposits carbon and oxygen on the surface, efforts were taken to minimize the amount. Using the model in Fig. 4, full coverage of aluminum would give a surface concentration of aluminum of 6% but since the Auger samples multiple layers, the observed saturation coverage of aluminum is lower.

	C	O	Al
Clean 4 × 2	1.8 ± 0.1%	0.2 ± 0.1%	0.0 ± 0.1%
O ₂	1.6 ± 0.1%	7.8 ± 0.1%	0.0 ± 0.1%
Clean 4 × 2	2.5 ± 0.1%	0.7 ± 0.1%	0.0 ± 0.1%
24 °C TMA	14.2 ± 0.2%	1.1 ± 0.1%	2.1 ± 0.3%
O ₂	16.9 ± 0.2%	1.2 ± 0.2%	2.5 ± 0.4%
Clean 4 × 2	3.3 ± 0.1%	0.6 ± 0.1%	0.0 ± 0.1%
280 °C TMA	12.5 ± 0.1%	1.1 ± 0.1%	2.4 ± 0.3%
O ₂	18.7 ± 0.1%	2.3 ± 0.1%	4.0 ± 0.1%

transition of aluminum, the intensity was estimated by the average of four different peak fittings. The total spectrum was either normalized to the In MNN transition or a low energy As peak that is just slightly higher in energy than the Al peak. The intensity was measured by taking the difference between the clean surface and the peak when the spectrums were aligned to either the valley just below or above the aluminum peak. The errors reported are from the standard deviation of these measured intensities along with the normalized noise, taken in an energy range with no peaks.

After dosing the clean 4 × 2 with TMA, an aluminum peak can be seen clearly.⁴² The percentages for the aluminum peak are difficult to extract because the peak overlaps other low energy In, Ga, and As peaks. An estimate of the aluminum concentrations are 2.07 ± 0.3% for the 24 °C and 2.36 ± 0.3% for the 280 °C dosed surfaces. With the model shown in Figure 4, if only the first layers were detected with AES the saturation coverage of aluminum would be ~6%; however, AES has an interaction depth ~1–2 nm. The carbon concentrations increased to over 12% for both the 24 °C and 280 °C TMA dose. The increase in carbon concentration is consistent with dissociative chemisorption of TMA to the surface breaking Al-methyl bonds, and chemisorption of the dissociated methyl to the surface introducing site blocking which restricts more aluminum bonding. Furthermore, the presence of methane or ethyl byproducts from the dosing source can produce an increase in the carbon contamination. With a constant flow or hot wall system, these byproducts maybe be reduced. The slight increase in aluminum coverage on the 280 °C surface is consistent with some of the chemisorbed methyl that blocks further dissociative chemisorption of TMA at 24 °C desorbing at 280 °C. During the 280 °C anneal in the preparation chamber, a large pressure burst is observed also consistent with further desorption.

After, the decapped 4 × 2 surface was exposed to 15 000 L of O₂, the oxygen increased to 7.8 ± 0.1% while the carbon remained below 3%.⁴² With the interaction volume

of AES, 7.8 ± 0.1% is a reasonable concentration for saturation coverage of oxygen on the In/Ga rich surface. It should be noted that the dosing conduit for the O₂ is a Teflon tube that is not baked, so background water may be present. After TMA dosing, the surfaces were again exposed to 15 000 L of O₂. The 24 °C TMA dosed surface which was subsequently annealed to 200 °C shows better resistance to oxygen and carbon contamination in comparison to the higher temperature TMA dosed surface. In STM, it was shown in Figure 1 that the higher temperature TMA dose on the 4 × 2 surface showed a wider row spacing allowing for more oxygen or carbon to react with dangling bonds or undercoordinated In, Ga, or As surface atoms. It was also shown, in Figure 5, that the higher temperature surface was pinned, which usually occurs when surface atoms have dangling bonds or are undercoordinated. The exposure of O₂ to the decapped clean surface decreases the low energy Ga and As peaks suggesting substrate oxidation.⁴² For the 25 °C or 280 °C TMA dosed surface, O₂ exposure induces a 5 eV shift of the aluminum peak to lower energy (dashed arrow), consistent with Al-O bonding⁴³ and less substrate oxidation. During the post deposition anneal the aluminum scavenges for oxygen, because the Al-O (511 ± 3 kJ mol⁻¹) bond is stronger than the As-O(481 ± 8 kJ mol⁻¹), Ga-O (353.5 ± 41.8 kJ mol⁻¹) or In-O (320 ± 41.8 kJ mol⁻¹) bonds.³⁵ It should be noted that the increase in aluminum concentration after O₂ exposure is due to the combination of the decrease in the low energy Ga peaks, a shift in the aluminum peak, and any residual TMA remaining in the ALD chamber.

The respective data for TMA and O₂ dosing on the InGaAs 2 × 4 surface is shown in Table II, see supplementary material for corresponding AES spectra.⁴² The aluminum concentration on the 2 × 4 surface show similarities to that of the 4 × 2 surface, consistent with a high nucleation density of aluminum breaking the surface As-dimers and makes two Al-As bonds. The AES atomic ratios for aluminum, carbon, and oxygen for the 24 °C and 280 °C dosed 2 × 4 surfaces support the results seen in STM showing nearly identical surface structures. The slight difference in aluminum concentration could be caused by a reduction of site blocking at elevated temperatures.

The decapped surface exposed to 15 000 L of O₂ shows an increase of oxygen to 5.1 ± 0.1% and the carbon concentration increased to 9.6 ± 0.1%, see top row AES spectra.⁴²

TABLE II. AES atomic ratios for InGaAs(001)-(2 × 4) surface and dosed surfaces. All clean surfaces show an atomic concentration of carbon <5% and oxygen <2% demonstrating the initial surface is extremely clean.

	C	O	Al
Clean 2 × 4	3.4 ± 0.1%	1.9 ± 0.1%	0.0 ± 0.1%
O ₂	9.6 ± 0.1%	5.1 ± 0.1%	0.0 ± 0.1%
Clean 2 × 4	4.8 ± 0.2%	2.0 ± 0.2%	0.0 ± 0.2%
24 °C TMA	9.7 ± 0.2%	1.9 ± 0.2%	1.9 ± 0.5%
O ₂	16.3 ± 0.3%	3.0 ± 0.3%	3.2 ± 0.9%
Clean 2 × 4	1.3 ± 0.2%	0.5 ± 0.1%	0.0 ± 0.1%
280 °C TMA	9.9 ± 0.1%	0.8 ± 0.1%	2.4 ± 0.4%
O ₂	10.6 ± 0.2%	0.9 ± 0.1%	2.3 ± 0.6%

The large oxygen and carbon concentration would correlate to a monolayer of reactance on the As-rich surface. This sensitivity to carbon is a clear difference between the 2×4 and 4×2 surfaces, it is expected that the 2×4 surface is more reactive and therefore more susceptible to background contamination. After TMA dosing, the surfaces were exposed to 15 000 L of O_2 . The 280 °C TMA dosed 2×4 surface shows a shift in the aluminum peak of 5 eV to lower energy, consistent with Al-O bonding. However, the 24 °C TMA dosed 2×4 surface resembles a decrease in the low energy Ga and As peaks similar to that of the oxidized decapped surface. The higher temperature TMA dosed surface, therefore, shows an improvement in protecting the reactive 2×4 surface from carbon or oxygen reactions.

SUMMARY

Atomic hydrogen cleaning is able to restore InGaAs(001)-(4×2) or (2×4) surface allowing for a gate-last or replacement-gate process. Formation of an electrical passive interface after TMA reaction on the InGaAs(001)-(4×2) requires atomic hydrogen cleaning around 380 °C followed by a PDA to 450–470 °C and initial seeding of TMA at sample temperature below 190 °C. The lower temperature seeding of InGaAs(001)-(4×2) with TMA shows a high nucleation density of aluminum that is less prone to oxygen reaction than a higher temperature seeding, while exhibiting an unpinned interface. Higher temperature (>190 °C) seeding with TMA on the 4×2 illustrates a non-ideal surface, which is more prone to carbon and oxygen contamination and exhibits a pinned interface. For the InGaAs(001)-(2×4), the atomic hydrogen cleaning and formation of an unpinned interface after TMA reaction can be achieved at a more ideal ALD temperature of 280 °C while maintaining a high nucleation density. Furthermore, the high temperature seeding shows an improvement in the protection of the surface in comparison to the lower temperature dosed surface from background carbon and oxygen consistent with formation of very strong As-Al-(CH₃)_x bonds. The advantage of the 4×2 gate-last process is that it can produce extremely flat surfaces but requires multiple temperature changes making it difficult to maintain a clean surface. On the other hand; the 2×4 gate-last process can be achieved at the same temperature as common Al₂O₃ growth temperatures, however, may have a higher surface roughness. For both the As-rich 2×4 and the In/Ga rich 4×2 , the surface chemistry of TMA is consistent with the dominant driving force being the formation of strong As-Al-As bonds which create an electrically passive interface and protect the surface from oxidation.

ACKNOWLEDGMENTS

This work was supported by National Science Foundation (NSF) under Grant Nos. NSF-DMR-0706243, SRC-NCRC-1437.003, and an Applied Materials GRC fellowship. The authors would also like to thank the on going collaborations within the SRC non-classical CMOS center.

- ¹J. Robertson and B. Falabretti, *J. Appl. Phys.* **100**, 014111 (2006).
- ²S. J. Bentley, M. Holland, X. Li, G. W. Paterson, H. P. Zhou, O. Ignatova, D. Macintyre, S. Thoms, A. Asenov, B. H. Shin, J. Ahn, P. C. McIntyre, and I. G. Thayne, *IEEE Electron Device Lett.* **32**, 494–496 (2011).
- ³M. Passlack, J. K. Abrokwah, R. Droopad, Z. Y. Yu, C. Overgaard, S. I. Yi, M. Hale, J. Sexton, and A. C. Kummel, *IEEE Electron Device Lett.* **23**, 508–510 (2002).
- ⁴E. J. Kim, L. Q. Wang, P. M. Asbeck, K. C. Saraswat, and P. C. McIntyre, *Appl. Phys. Lett.* **96**, 012906 (2010).
- ⁵Y. Q. Wu, M. Xu, R. S. Wang, O. Koybasi, and P. D. Ye, 2009 IEEE International Electron Devices Meeting (IEDM), 2009, pp. 1–4.
- ⁶E.-H. Roman, H. Yoontae, and S. Susanne, *J. Appl. Phys.* **108**, 124101 (2010).
- ⁷C. H. Diaz, K. Goto, H. T. Huang, Y. Yasuda, C. P. Tsao, T. T. Chu, W. T. Lu, V. Chang, Y. T. Hou, Y. S. Chao, P. F. Hsu, C. L. Chen, K. C. Lin, J. A. Ng, W. C. Yang, C. H. Chen, Y. H. Peng, C. J. Chen, C. C. Chen, M. H. Yu, L. Y. Yeh, K. S. You, K. S. Chen, K. B. Thei, C. H. Lee, S. H. Yang, J. Y. Cheng, K. T. Huang, J. J. Liaw, Y. Ku, S. M. Jang, H. Chuang, and M. S. Liang, 2008 IEEE International Electron Devices Meeting (IEDM), 2008, pp. 1–4.
- ⁸T. Tomimatsu, Y. Goto, H. Kato, M. Amma, M. Igarashi, Y. Kusakabe, M. Takeuchi, S. Ohbayashi, S. Sakashita, T. Kawahara, M. Mizutani, M. Inoue, M. Sawada, Y. Kawasaki, S. Yamanari, Y. Miyagawa, Y. Takeshima, Y. Yamamoto, S. Endo, T. Hayashi, Y. Nishida, K. Horita, T. Yamashita, H. Oda, K. Tsukamoto, Y. Inoue, H. Fujimoto, Y. Sato, K. Yamashita, R. Mitsuhashi, S. Matsuyama, Y. Moriyama, K. Nakanishi, T. Noda, Y. Sahara, N. Koike, J. Hirase, T. Yamada, H. Ogawa, M. Ogura, 2009 Symposium on VLSI Technology, 2009, pp. 36–37.
- ⁹F. Arnaud, J. Liu, Y. M. Lee, K. Y. Lim, S. Kohler, J. Chen, B. K. Moon, C. W. Lai, M. Lipinski, L. Sang, F. Guarin, C. Hobbs, P. Ferreira, K. Ohuchi, J. Li, H. Zhuang, P. Mora, Q. Zhang, D. R. Nair, D. H. Lee, K. K. Chan, S. Satadru, S. Yang, J. Koshy, W. Hayter, M. Zaleski, D. V. Coolbaugh, H. W. Kim, Y. C. Ee, J. Sudijono, A. Thean, M. Sherony, S. Samavedam, M. Khare, C. Goldberg, and A. Steegen, 2008 IEEE International Electron Devices Meeting (IEDM), 2008, pp. 1–4.
- ¹⁰K. Choi, H. Jagannathan, C. Choi, L. Edge, T. Ando, M. Frank, P. Jamison, M. Wang, E. Cartier, S. Zafar, J. Bruley, A. Kerber, B. Linder, A. Callegari, Q. Yang, S. Brown, J. Stathis, J. Iacoponi, V. Paruchuri, and V. Narayanan, 2009 Symposium on VLSI Technology, 2009, pp. 138–139.
- ¹¹Y. Taur and T. H. Ning, *Fundamentals of Modern VLSI Devices* (Cambridge University Press, Cambridge/New York, 2009).
- ¹²P. Packan, S. Akbar, M. Armstrong, D. Bergstrom, M. Brazier, H. Deshpande, K. Dev, G. Ding, T. Ghani, O. Golonzka, W. Han, J. He, R. Heussner, R. James, J. Jopling, C. Kenyon, S. H. Lee, M. Liu, S. Lodha, B. Mattis, A. Murthy, L. Neiberg, J. Neirynck, S. Pae, C. Parker, L. Pipes, J. Sebastian, J. Seiple, B. Sell, A. Sharma, S. Sivakumar, B. Song, A. St. Amour, K. Tone, T. Troeger, C. Weber, K. Zhang, Y. Luo, and S. Natarajan, 2009 IEEE International Electron Devices Meeting (IEDM), 2009, pp. 1–4.
- ¹³X. Li, S. Bentley, H. McLelland, M. C. Holland, H. Zhou, S. Thoms, D. S. Macintyre, and I. G. Thayne, *J. Vac. Sci. Technol. B* **28**, C6L1–C6L5 (2010).
- ¹⁴M. Milojevic, F. S. Aguirre-Tostado, C. L. Hinkle, H. C. Kim, E. M. Vogel, J. Kim, and R. M. Wallace, *Appl. Phys. Lett.* **93**, 202902 (2008).
- ¹⁵C. L. Hinkle, A. M. Sonnet, E. M. Vogel, S. McDonnell, G. J. Hughes, M. Milojevic, B. Lee, F. S. Aguirre-Tostado, K. J. Choi, H. C. Kim, J. Kim, and R. M. Wallace, *Appl. Phys. Lett.* **92**, 071901 (2008).
- ¹⁶C. H. Chang, Y. K. Chiou, Y. C. Chang, K. Y. Lee, T. D. Lin, T. B. Wu, M. Hong, and J. Kwo, *Appl. Phys. Lett.* **89**, 242911 (2006).
- ¹⁷A. D. Carter, W. J. Mitchell, B. J. Thibeault, J. J. M. Law, and M. J. W. Rodwell, *Appl. Phys. Express* **4**, 091102 (2011).
- ¹⁸M. Radosavljevic, G. Dewey, J. M. Fastenau, J. Kavalieros, R. Kotlyar, B. Chu-Kung, W. K. Liu, D. Lubyshev, M. Metz, K. Millard, N. Mukherjee, L. Pan, R. Pillarisetty, W. Rachmady, U. Shah, and R. Chau, 2010 IEEE International Electron Devices Meeting (IEDM), 2010, pp. 1–4.
- ¹⁹W. Melitz, J. Shen, T. Kent, A. C. Kummel, and R. Droopad, *J. Appl. Phys.* **110**, 013713 (2011).
- ²⁰Y. Hwang, R. Engel-Herbert, and S. Stemmer, *Appl. Phys. Lett.* **98**, 052911 (2011).
- ²¹A. Molle, L. Lamagna, C. Grazianetti, G. Brammertz, C. Merckling, M. Caymax, S. Spiga, and M. Fanciulli, *Appl. Phys. Lett.* **99**, 193505 (2011).
- ²²J. B. Clemens, E. A. Chagarov, M. Holland, R. Droopad, J. A. Shen, and A. C. Kummel, *J. Chem. Phys.* **133**, 154704 (2010).

- ²³J. Shen, D. L. Winn, W. Melitz, J. B. Clemens, and A. C. Kummel, *ECS Trans.* **16**, 463–468 (2008).
- ²⁴R. M. Feenstra, *Surf. Sci.* **300**, 965–979 (1994).
- ²⁵J. A. Strosio, R. M. Feenstra, D. M. Newns, and A. P. Fein, *J. Vac. Sci. Technol. A* **6**, 499–507 (1988).
- ²⁶W. Mönch, *Semiconductor Surfaces and Interfaces* (Springer-Verlag, Berlin/New York, 1995).
- ²⁷P. Martensson and R. M. Feenstra, *Phys. Rev. B* **39**, 7744–7753 (1989).
- ²⁸J. Shen, J. B. Clemens, E. A. Chagarov, D. L. Feldwinn, W. Melitz, T. Song, S. R. Bishop, A. C. Kummel, and R. Droopad, *Surf. Sci.* **604**, 1757–1766 (2010).
- ²⁹N. Ikoma and S. Ohkouchi, *Jpn. J. Appl. Phys., Part 1* **34**, 5763–5767 (1995).
- ³⁰M. M. Sung and J. W. Rabalais, *Surf. Sci.* **356**, 161–170 (1996).
- ³¹E. J. Kim, E. Chagarov, J. Cagnon, Y. Yuan, A. C. Kummel, P. M. Asbeck, S. Stemmer, K. C. Saraswat, and P. C. McIntyre, *J. Appl. Phys.* **106**, 124508 (2009).
- ³²S. J. Pearton, *Mater. Sci. Eng., B* **10**, 187–196 (1991).
- ³³M. Yamada, Y. Ide, and K. Tone, *Jpn. J. Appl. Phys., Part 2* **31**, L1157–L1160 (1992).
- ³⁴F. S. Aguirre-Tostado, M. Milojevic, C. L. Hinkle, E. M. Vogel, R. M. Wallace, S. McDonnell, and G. J. Hughes, *Appl. Phys. Lett.* **92**, 171906 (2008).
- ³⁵J. A. Kerr, *CRC Handbook of Chemistry and Physics 1999-2000: A Ready-Reference Book of Chemical and Physical Data*, edited by D. R. Lide (CRC, Boca Raton, FL, 2000).
- ³⁶D. L. Feldwinn, J. B. Clemens, J. Shen, S. R. Bishop, T. J. Grassman, A. C. Kummel, R. Droopad, M. Passlack, *Surf. Sci.* **603**, 3321–3328 (2009).
- ³⁷G. Goryl, D. Toton, M. Goryl, N. Tomaszewska, and J. J. Kolodziej, *Surf. Sci.* **605**, 2073–2081 (2011).
- ³⁸C. Kumpf, L. D. Marks, D. Ellis, D. Smilgies, E. Landemark, M. Nielsen, R. Feidenhans, J. Zegenhagen, O. Bunk, J. H. Zeysing, Y. Su, and R. L. Johnson, *Phys. Rev. Lett.* **86**, 3586–3589 (2001).
- ³⁹M. Akazawa and H. Hasegawa, *Appl. Surf. Sci.* **256**, 5708–5713 (2010).
- ⁴⁰W. Melitz, J. Shen, S. Lee, J. S. Lee, A. C. Kummel, R. Droopad, and E. T. Yu, *J. Appl. Phys.* **108**, 023711 (2010).
- ⁴¹P. W. Palmberg, G. E. Riach, R. E. Weber, and N. C. Macdonald, *Handbook of Auger Electron Spectroscopy* (Physical Electronics Industries, Inc., Minnesota, 1972).
- ⁴²See supplementary material at <http://dx.doi.org/10.1063/1.4704126> for normalized 3 keV AES spectra for TMA dosing and O₂ on InGaAs 4 × 2 surface and normalized 3 keV AES spectra for TMA dosing and O₂ on InGaAs 2 × 4 surface.
- ⁴³A. Mesarwi and A. Ignatiev, *J. Appl. Phys.* **71**, 1943–1948 (1992).